Colloid Polym Sci (2012) 290:953–964
DOI 10.1007/s00396-012-2615-0

ORIGINAL CONTRIBUTION

Experimental research and DPD simulation on the interaction between an ethoxy-modified trisiloxane and F127

Jinyu Pang · Guiying Xu · Yebang Tan

Received: 12 October 2011 / Revised: 13 January 2012 / Accepted: 20 February 2012 / Published online: 8 March 2012

Abstract The interactions between surfactants and polymers are widely investigated due to favorable changes on properties in their mixtures. Silicone surfactants and pluronic copolymers, both having low toxicity, are used in the detergent, cosmetics, medical, and pharmaceutical fields. Their mixture may gain better performance in their further applications. Therefore, we investigated the interaction between an ethoxy-modified trisiloxane (a silicone surfactant named Ag-64) and a block polyether F127 in this paper. From aggregation behavior of Ag-64 and F127, the formation mechanism and conformation of the aggregates were proposed based on experiments and dissipative particle dynamics (DPD) simulation. The surface activity and aggregation behavior of Ag-64 are affected by F127 in aqueous solutions. As the amounts of added Ag-64 increase, two types of aggregates (Ag-64/F127 aggregate with F127 as skeleton and the "pearl- necklace" aggregate in which Ag-64 micelles are strung along F127 chain) form successively. At higher polymer concentration, F127 twists together to form a coil/cluster aggregate with Ag-64. The results of DPD simulation approve that two main factors, the hydrophobic association and twist of F127 coil, contribute to the formation of different aggregates of Ag-64 and F127.

Keywords Silicone surfactant · F127 · Mixture · DPD simulation

J. Pang · G. Xu (✉) · Y. Tan
Key Laboratory of Colloid and Interface Chemistry,
Ministry of Education, Shandong University,
Jinan 250100, People's Republic of China
e-mail: xuguiying@sdu.edu.cn

Introduction

Mixtures of polymers and surfactants in solutions have achieved considerable interest. As a consequence of their interaction, a polymer may affect the aggregation behavior of a surfactant while its adsorption characteristics will be also influenced [1, 2]. This is technically important because the mixed systems may provide a way of tailoring properties through simple composition variations, thus new structures may be obtained by changing the system composition rather than through synthesis of new materials [3]. Furthermore, PEO-PPO-PEO block polyethers have been widely used in detergency and pharmaceutical bioprocessing because of low toxicity and high biocompatibility [4, 5]. Therefore, there is much research on the interaction between PEO-PPO-PEO block polyethers and surfactants [6–8]. Our group also carried out some investigations in this subject [9–11].

The binary mixtures contained nonionic surfactants have been described as non-interacting or very weakly interacting [12, 13]. However, Feitosa et al found that poly(ethylene glycol) (PEG) can interact with the nonionic surfactant octaethylene glycol dodecyl ether ($C_{12}E_8$) to form aggregates, which possibly consists of one or more $C_{12}E_8$ micelles surrounded by a PEG chain [13]. And micellar clusters of pentaethylene glycol dodecyl ether ($C_{12}E_5$) are formed within the poly(ethylene oxide) (PEO) coils, and its aggregation number increases with the amount of PEO at a constant $C_{12}E_5$ concentration [14]. A triblock polyether $EO_{20}PO_{68}EO_{20}$ (P123) and hexaoxyethylene dodecyl ether ($C_{12}E_6$) also show strong interactions, and they form mixed micelles at the critical micelle concentration (CMC) which is lower than that of pure $C_{12}E_6$ in aqueous solution [15].

Triblock polyether $EO_{97}PO_{69}EO_{97}$ (Pluronic F127) has been used in medical and pharmaceutical fields, such as in arterial embolization [16], drug delivery [17, 18] and overdose [19], and blood compatibility [20]. F127 interacts with $C_{12}E_6$ [21] as well as TX-100 [22] to form mixed micelle or complex. Silicone surfactant also has low toxicity and favorable biocompatibility [23], thus it is widely applied to these fields. We also found that the mixture of F127 and Ag-64 has a synergistic effect on dispersing carbon nanotubes in water [24]. Therefore, the investigation on the mixture of PEO-PPO-PEO polyether and silicone surfactant may lead to a new approach for their further applications.

One of the fundamental requirements in understanding the behavior of these mixtures is the knowledge of the interaction mechanism and binding mode, which are critical for solution properties and further application. Dissipative particle dynamics (DPD) is especially appropriate for the simulation of polymer–surfactant aggregation [25, 26]. In our previous research, DPD simulation has been successfully applied in studying the aggregation of surfactants and polymers [11, 27–29]. Herein, the interaction between an ethoxy-modified trisiloxane Ag-64 and F127 was investigated by both experiments and DPD simulation.

Experimental

Materials

The silicone surfactant Ag-64 and Pluronic F127 are the same as used in our previous work [24]. Their chemical structures are shown in Scheme 1. They were both used as received without further purification. Water in the experiments was triply distilled by a quartz water purification system.

Surface tension measurement

The surface tension (γ) of system was measured on a Krűss K12 Processor Tensiometer by plate method of Wilhelmy. Target solutions were thermostated at 25.0 °C for 15 min before measuring. The CMC was obtained by plotting surface tension as a function of surfactant concentration.

Fluorescence spectroscopy measurement

Steady-state fluorescence measurements were carried out on a RF-540 Spectrofluorimeter (Japan), and pyrene purchased from Sigma was used as probe. A methanol solution with 1×10^{-4} mol·dm^{-3} pyrene was put into a series of glass tubes, and methanol was evacuated by ventilation with nitrogen. The aqueous solutions of surfactants were then added into the tubes, in which the concentration of pyrene was 6×10^{-7} mol·dm^{-3}. After sonication for 30 min in an ultrasonic bath, the solutions were kept at room temperature for 2 h before spectroscopic measurement. The emission spectra of the probe were recorded at wavelength range from 350 to 550 nm. Wavelength of 335 nm was selected for excitation, and the bandwidths were set to 10 nm for excitation and 2.5 nm for emission. The information of polarity in micelle was obtained by the ratio of the fluorescent intensity at two peaks, the first vibronic peak at 373 nm (I_1) and the third vibronic peak at 384 nm (I_3).

Dynamic light scattering measurement

The dynamic light scattering experiments were performed using a commercial goniometer (DAWN HELEOS made by Wyatt corporation) equipped with a laser (wavelength λ= 658 nm) at 90° scattering angle.

Different quantities of Ag-64 and F127 were firstly dissolved into sealed tubes with triply distilled water and stored for 1 week. Then, the target solutions were filtered once through 0.2-μm Millipore filters directly into the glass bottle for light scattering measurement and sealed until used.

DPD simulation

DPD is a stochastic simulation technique introduced by Hoogerbrugge and Koelman [30] and often used to simulate complex fluid dynamical behaviors. The simulation strategy is to group atoms together into single "bead" and uses these centers of mass as new simulation entities. A modified Velocity–Verlet algorithm [31] is adopted to integrate the Newton's equation of motion. The position r_i and momentum p_i of particles on representation of next position,

Scheme 1 The structures of **a** Ag-64 ($n\leq18$) and **b** F127

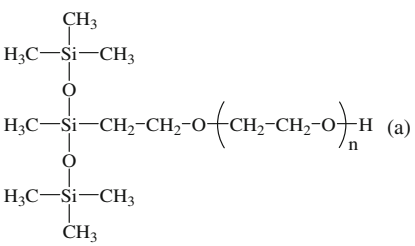

(a)

$(C_2H_4O)_{97}(C_3H_6O)_{69}(C_2H_4O)_{97}$ (b)

Linear MW: 12600 EO wt% ≈ 70%

velocity, and force on a soft particle are calculated from the following equations:

$$dr_i = \left(\frac{p_i}{m}\right)dt \tag{1}$$

$$dp_i = \sum_j \Omega_{ij}\hat{r}_{ij}dt \tag{2}$$

$$\Omega_{ij} = \omega(r_{ij})\left[a_{ij} + \sigma\theta_{ij} - \frac{\sigma^2}{2kT}\omega(r_{ij})\hat{r}_{ij}\upsilon_{ij}\right] \tag{3}$$

where a_{ij} is a maximum repulsion between particle i and particle j, $r_{ij}=r_j-r_i$ and $\hat{r}_{ij}=r_{ij}/|r_{ij}|$. ω is r-dependent weight function and $\omega(r_{ij})=(1-r)$ for $r<1$, $\omega(r_{ij})=0$ for $r>1$. σ is the noise amplitude, $\sigma^2=2\gamma$kT (γ, k, and T are friction coefficient, Boltzmann's constant, and equilibrium temperature). θ and υ are the angle between the three connected DPD beads and velocity vector of a particle. Conservative force, random force, and dissipative force are represented by the three terms in the square brackets of Eq. 3, and the latter two acting as heat sink and heat source combine to be a thermostat.

In DPD simulation, two critical conditions should be satisfied, the liquid compressibility which determines the free energy change associated to density fluctuations and the mutual solubility expressed by the Flory–Huggins parameters. To keep the compressibility of water at room temperature, the repulsion parameter in Eq. 3 is calculated according to [32]:

$$a_{ii} = \frac{75k_BT}{\rho},\ \rho = 3 \tag{4}$$

where a_{ii} is the repulsion parameter between particles of the same type and ρ is the particle density.

The repulsion between different beads is also stronger than that between the same beads. It is indicated that different types of beads usually tend to segregate, such as a water molecule and a monomer of polymer. The value of the repulsion between different types of beads is linearly related to the χ-parameter, and it is easy to obtain from the following equation [32]:

$$a_{ij} \approx a_{ii} + 3.27\chi_{ij},\ \rho = 3 \tag{5}$$

Ag-64 is represented by five beads, in which the head contains two beads and the tail has three beads. They are tied together by a harmonic spring, and water molecule is expressed by one bead. From the method by van Vlimmeren et al. [33], the chain of F127 $(EO)_{97}(PO)_{69}(EO)_{69}$ is defined as $A_{23}B_{21}A_{23}$ (A=PEO, B=PPO). The Flory–Huggins parameters between two simulated objects are firstly calculated and then transformed into DPD repulsion parameters via Eqs. 4 and 5.

The simulation system was carried out in a cubic cell of 15 R_c×15 R_c×15 R_c, where R_c is the cut-off radius. The spring constant between different beads is chosen to be 4.0 according to Groot's work [25]. To assure the system have achieved equilibrium, 20,000 simulation steps were performed before the results were analyzed, which is confirmed to be a sufficient simulation time [34].

Since Ag-64, F127 and water molecule were selected to be the simulated targets; the mixing free energies and Flory–Huggins parameters (χ) could be obtained by solubility parameter as following: [35]

$$\chi_{sp} = (\delta_s - \delta_p)^2 V_s/RT \tag{6}$$

where δ_s and δ_p are Scatchard–Hildebrand solubility parameters of solvent and surfactant, respectively, and V_s is the molar volume of solvent.

The Flory–Huggins parameters (χ_{ij}) were transformed into DPD parameters (a_{ij}), as shown in Table 1. Using these parameters, DPD calculations were carried out. The interaction parameters among SiO, PEO, PPO, and H_2O at 298K were listed in Table 1.

Results and discussion

The effect of F127 on the surface activity of Ag-64

From the surface tension isotherm of Ag-64 in Fig. 1, the curve continues to decrease until a break and then the surface tension values remain constant with a further increase of Ag-64 concentration. The CMC of Ag-64 is 85 mg·L^{-1} confirmed by the break of surface tension curve. There is no minimum followed by a rise around CMC, which indicates no higher surface activity substance in this sample. With the increase of Ag-64 concentration, more and more Ag-64 molecules adsorb on the surface of solution until the surface is occupied completely. The lowest value in the surface tension represents adsorption saturation of Ag-64 at the surface. As Ag-64 concentration is further increased, Ag-64 molecules begin to form aggregates in the solution, and the surface tension reduces no more. Different from the properties of Ag-64, there are two breaks in the surface tension isotherm of F127, which is common for PEO-PPO-PEO copolymers. Because of broad molecular

Table 1 The interaction parameters a_{ij} in DPD simulation

a_{ij}	H_2O	SiO	PEO	PPO
H_2O	25.0	45.0	25.9	30.0
SiO	45.0	25.0	25.8	25.1
PEO	25.9	25.8	25.0	34.8
PPO	30.0	25.1	34.8	25.0

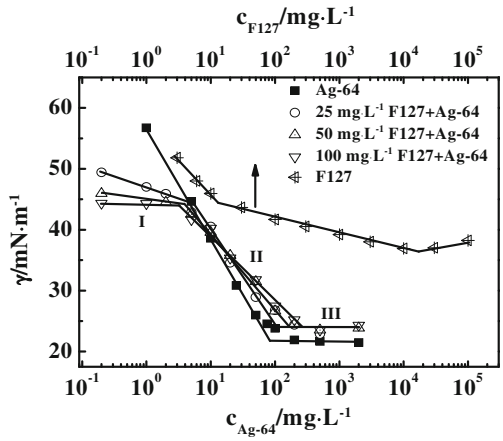

Fig. 1 Surface tension isotherms of Ag-64 aqueous solutions with different amounts of F127 at 25 °C

weight distribution, unimer or oligomer forms at the concentration below CMC [36, 37]. The CMC of F127 should be determined by the second break, which is 1.70×10^4 mg L^{-1} comparable to the value reported [38].

The addition of F127 to Ag-64 solutions also leads to two breaks (T_1 and T_2) in the surface tension isotherms, and it can be predicted that the F127/Ag-64 complex is formed according to Flomer's work [39]. Increasing the polymer concentration, the surface tension isotherms shift to higher surfactant concentrations, which is similar to the results reported by other researchers [40, 41]. The two breaks divide the surface tension isotherm into three regions as shown in Fig. 1 (regions I, II, and III). T_1 below CMC is denoted as critical aggregation concentration (CAC), which represents the onset of the association of Ag-64 and F127 in the bulk phase. The second break (T_2) above CMC is the concentration at which F127 is saturated with Ag-64. Specific parameters of surface properties are shown in Table 2. T_1 value does not change obviously with F127 amount, which is consistent with other reported results [42, 43]. It only decreases slightly with the increasing amounts of F127. This result indicates the surfactant readily associates with the polymer as there are more amounts of polymer in solutions. T_2 value increases dramatically with the amounts of added F127. It is suggested that more Ag-64 bind to F127 so that aggregates form in the solution at higher concentrations.

Table 2 Surface properties of Ag-64 with different amounts of added F127

c_{F127}, mg·L^{-1}	T_1, mg·L^{-1}	T_2, mg·L^{-1}	γ_{CMC}, mN m^{-1}	T_2-cmc[a], mg L^{-1}
25	5	106	24.0	21
50	4	170	24.0	85
100	3	265	24.0	160

[a] CMC of pure Ag-64 aqueous solution

The surface tension isotherms of the mixtures are between those of pure Ag-64 and F127, except the region below CAC. In region I, the surface tension value of the binary mixture is lower than that of the individual Ag-64 but similar to that of individual F127. Co-adsorption of Ag-64 and F127 may take place at the air/water surface. In region II, more and more Ag-64 binds to F127, leading to continuously decreased surface tension until a break. There is an increase of γ_{CMC} after adding F127 to Ag-64 solutions, and it does not change with F127 amounts. This may be caused by the fact that Ag-64 competes with F127 to adsorb at the surface, while F127 at the surface is not completely replaced by Ag-64. The value of T_2-cmc was also calculated, and it correlates linearly with F127 amounts with a slope of 2.1, which shows the bound amount of Ag-64 to F127. As mentioned above, the addition of F127 has an influence on the surface properties of Ag-64 solution.

The effect of F127 on the polarity in the micelle of Ag-64

As pyrene is employed as a probe, the fluorescence spectrum of pyrene monomer consists of five vibronic peaks. The ratio of the relative intensities of the first to the third vibronic band (I_1/I_3) is largely dependent on the polarity of microenvironment, and it is defined as a "hydrophobic index" [44, 45]. The low value of I_1/I_3 indicates that the probe is in a hydrophobic environment, and the high value shows an environment of a polar water-like solvent. Therefore, it can be used to confirm whether Ag-64/F127 aggregates have formed. The variation of I_1/I_3 with increasing Ag-64 concentrations was shown in Fig. 2. Firstly, the curves have no change with increasing Ag-64 concentration, then decrease steeply, and finally reach a plateau, which caused two breaks (p_1 and p_2). The curves corresponding to the systems contained F127 are beyond the curve of individual surfactant system. It is inferred from higher I_1/I_3 value in the presence of F127 that the probe is in a relatively polar environment and the arrangements of the aggregates are looser. It is likely that Ag-64 may adsorb along the chain

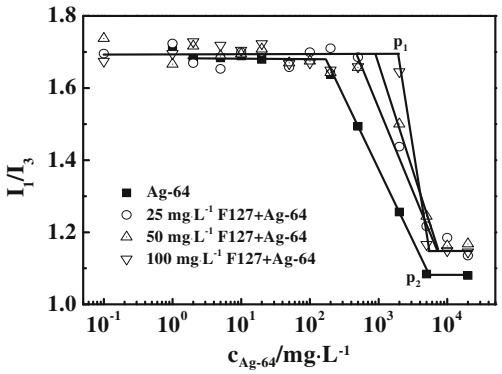

Fig. 2 The variation of I_1/I_3 as a function of Ag-64 concentrations

of F127. Aggregates with looser arrangements may be a coil/cluster aggregate in which Ag-64 clusters are twisted by F127 chains. It is also discovered that the first break p_1 in the mixed systems is at higher concentration of Ag-64 as more amounts of F127 are added. Therefore, regular Ag-64 micelles form at higher concentration in the presence of F127. This is in agreement with the results of surface tension measurement.

The hydrodynamic radius and size distribution of Ag-64/F127 aggregates

From the results of the surface tension isotherms in the presence of F127, two breaks divide the curves into three regions, where different aggregates are likely to form. Therefore, 1, 30, 100, 200, and 400 mg L^{-1} Ag-64 solutions with different amounts of F127 were chosen to investigate the aggregate behavior of the mixtures. Hydrodynamic radii of the aggregates were obtained via dynamic light scattering (DLS) measurement as shown in Fig. 3.

No aggregate is discovered below 100 mg L^{-1} Ag-64 or 50 mg L^{-1} F127 in individual surfactant or polymer system. The addition of F127 into Ag-64 solutions affects the hydrodynamic radius distribution of aggregates obviously. In the presence of 25 mg L^{-1} F127, the size of aggregate almost has no change as the concentration of Ag-64 is above 100 mg L^{-1}. This phenomenon also occurs as the surfactant concentration is higher than 200 or 300 mg L^{-1} in the system contained 50 or 100 mg L^{-1} F127, respectively. This trend is consistent with T_2 variation in the presence of different amounts of F127. Above these concentrations, F127 is saturated by Ag-64.

In region I, no aggregate is detected in the solution containing 1 mg L^{-1} Ag-64 and 25 mg L^{-1} F127, as well as at the same concentrations in individual Ag-64 or F127 solutions. As the concentration of Ag-64 is fixed to 1 mg L^{-1}, the small size of aggregates form in the presence of larger amounts of F127. Additionally, the size distribution is comparable to that in the individual polymer system at the same concentration. This result could be evidence to prove the aggregate is the unimer or oligomer of F127. The variation of size distribution in region II is more complicated. At higher Ag-64 concentration of 30 mg L^{-1}, higher and broader hydrodynamic radius distribution may be related to Ag-64/F127 aggregates with F127 as skeleton. As a small amount of F127 is added (25 mg L^{-1}) into Ag-64 solutions, the aggregate size gradually increases with Ag-64 concentration. In this case, F127 is readily saturated by Ag-64 through the interactions between non-polar segments, the PPO groups of F127, and SiO groups of Ag-64. With the addition of high amounts of F127 (100 mg L^{-1}), there is a

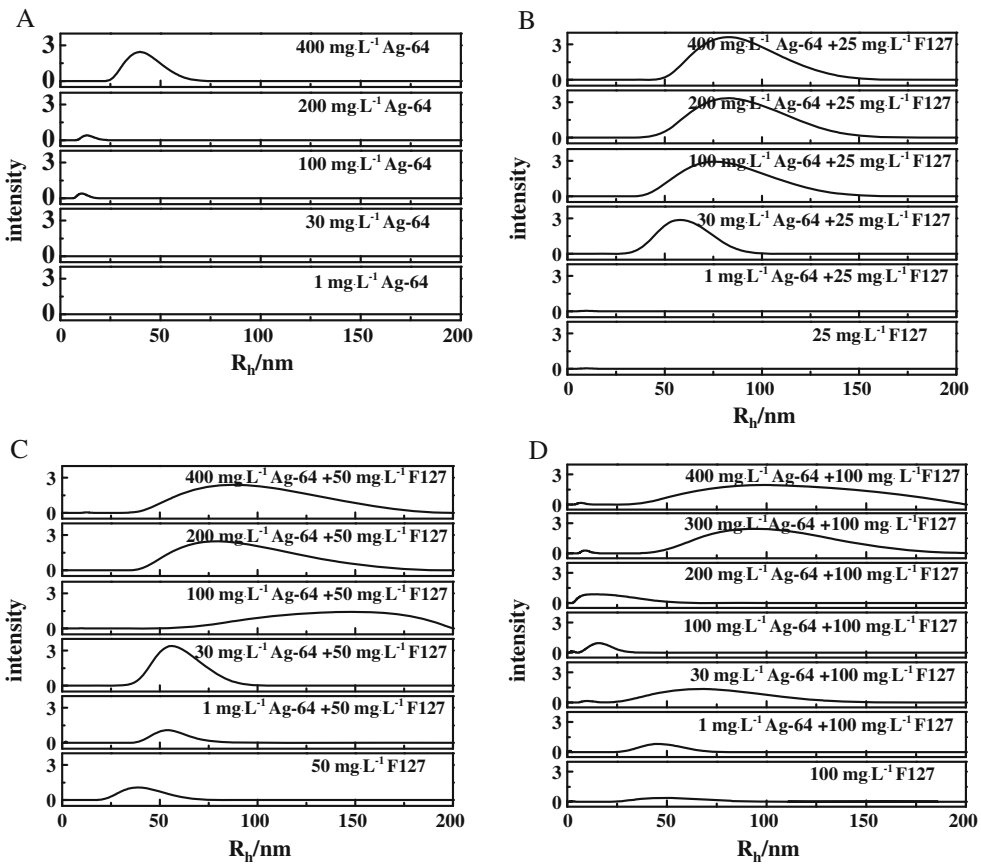

Fig. 3 The hydrodynamic radius distribution of Ag-64 micelle in the **a** absence and presence of **b** 25, **c** 50, **d** 100 mg L^{-1} F127 as determined by DLS

pronounced breakdown of aggregates as shown in Fig. 3d. This phenomenon is also observed in other polymer–surfactant systems [46–48]. As more and more Ag-64 binds to F127, the Ag-64/F127 aggregates disintegrate into small ones. The hydrodynamic radius distribution of the small aggregate after breakdown is similar to the one in the pure Ag-64 solution at the same concentration, which suggests that F127 coil may thread through Ag-64 micelles in this aggregate. In region III, the aggregates in each Ag-64/F127 system are much larger than those in individual Ag-64 or F127 solutions at the same concentration. They are likely to be a coil/cluster aggregate, in which small Ag-64 clusters are within F127 coils. The size distribution is very wide, and other aggregates may coexist with the coil/cluster aggregate, which should be the unimer or oligomer of F127, or a small F127-rich complex with Ag-64.

Apparently, the amounts of added F127 have an effect on the hydrodynamic radius distribution of aggregates. With an increase of the F127 content, Ag-64 firstly form an aggregate with F127 as skeleton, and then a coil/cluster aggregate forms in which Ag-64 clusters may aggregate on F127 coils. As the concentration of F127 is 100 $mg \cdot L^{-1}$, another type of aggregate is discovered in the region between T_1 and T_2, in which F127 chain may thread through Ag-64 micelles.

DPD simulation

Conformation of Ag-64/F127 aggregate

Although we have obtained much information on the aggregate behavior of Ag-64/F127 mixtures via experimental investigations, the microstructures of the aggregates are difficult to access directly in these methods but available through computer simulations [49]. Because the target systems in above experiments were still dilute solutions, Ag-64 at higher volume fraction was not considered in this paper. Mixtures of Ag-64 and F127 at different volume fractions (φ) below 0.08 were carried out in DPD simulations. Selected volume fractions are difficult to coincide with the concentrations in experiments, but it could hopefully provide a fundamental mechanism for the formation of Ag-64/F127 aggregates.

The configurations of Ag-64/F127 mixtures at different simulation steps are shown in Fig. 4. To further confirm the structure of Ag-64/F127 aggregates, distribution profiles of different components were displayed in Fig. 5. The profile image can directly show the location of a segment or molecule on a slice of the supercell. In the absence of Ag-64, F127 coils twist partially rather than form aggregates. As φ_{F127} is 0.02 and $\varphi_{Ag\text{-}64}$ is 0.01, the SiO groups of Ag-64 interact with the PPO groups of F127, forming an aggregate with F127 as skeleton. This structure can be clearly observed in Fig. 5a, which shows that the locations of SiO and PO segments overlap each other, indicating interactions between them. More Ag-64 molecules bind to F127 at higher $\varphi_{Ag\text{-}64}$, and finally, a coil/cluster aggregate appears, corresponding to the structure shown in Fig. 5c. All the SiO and PO segments aggregate together and locate at the same place. EO chains of F127 shrink, not like the situation in Fig. 5a where they stretch in water. The coil/cluster aggregate becomes larger with a further increase of Ag-64 content. Fixing φ_{F127} to 0.05, above two types of aggregates are also observed at low and high Ag-64 content. It is notable that another type of aggregate forms as $\varphi_{Ag\text{-}64}$ is 0.03 (as shown in Fig. 4b (c)), in which F127 coil threads through several Ag-64 micelles like a pearl necklace. Its distribution profile is displayed in Fig. 5b. There are Ag-64 molecules aggregated on the long polymer chain in different positions, which is like a pearl necklace. Additionally, this aggregate is smaller compared with the one forming in the solution with the same surfactant content but lower polymer content (as shown in Fig. 4a (c)). These results are in good agreement with above experimental results. At further, higher φ_{F127} (Fig. 4c (f)), all the Ag-64 molecules adsorb onto the F127, and most F127 is saturated with bound Ag-64. The other unsaturated F127 aggregates into a F127-rich complex with a few Ag-64 adsorbed on, and they coexist with the coil/cluster aggregates. Figure 5d shows the aggregation behavior in this case by the distribution profile. Large amounts of surfactant molecules adsorb on shrunk polymer chains, and a coil/cluster aggregate appears. Other polymer molecules form a complex with a few surfactant molecules adsorbed on.

Core size of Ag-64/F127 aggregate in the absence and presence of F127

In our simulations, the volume of Ag-64/F127 aggregate cannot be calculated accurately. However, the core size could express the variation trend of the volumes of Ag-64/F127 aggregates, which can be obtained through the software. The variation in the core size (the volume of the core defined by the siloxane parts of Ag-64) is shown in Fig. 6. At low $\varphi_{Ag\text{-}64}$, there are a few surfactant molecules in individual Ag-64 solution, and they have a tendency to aggregate together to form the premicelle. Its core size was also calculated in the same way.

As φ_{F127} is invariable, the aggregate becomes larger with the increase of $\varphi_{Ag\text{-}64}$. In the presence of F127, the aggregates are larger than these in pure Ag-64 solutions. When φ_{F127} is 0.02 and $\varphi_{Ag\text{-}64}$ is less than 0.03, the core size value is almost the same as that in pure Ag-64 solution. As φ_{F127} and $\varphi_{Ag\text{-}64}$ are both low, Ag-64 molecules aggregate on F127 chain with F127 as a skeleton, thus the core size without and with F127 are similar. At higher $\varphi_{Ag\text{-}64}$ and φ_{F127}, the coil/cluster aggregate forms, resulting in a bigger

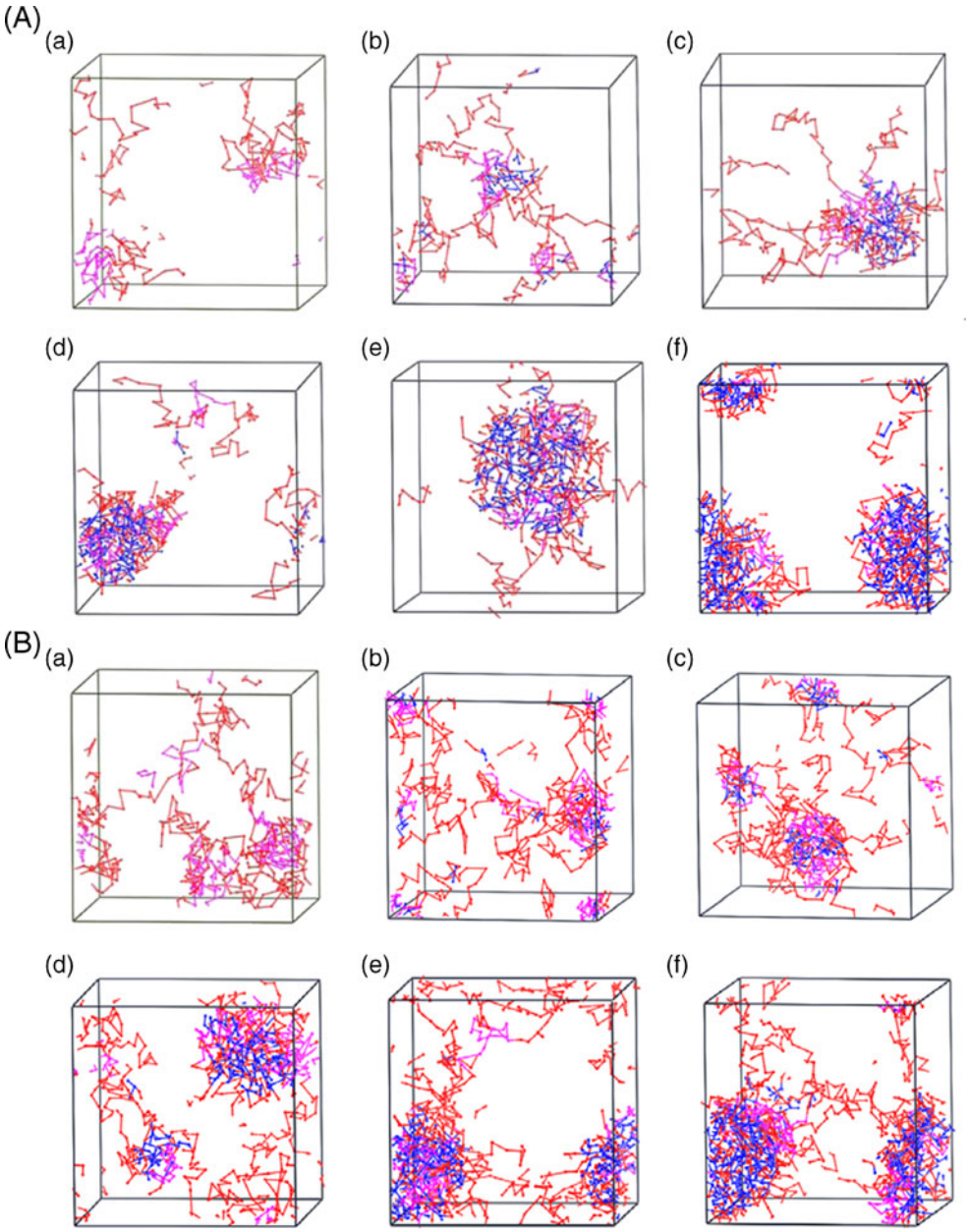

Fig. 4 The aggregate configurations of *a* 0, *b* 0.01, *c* 0.02, *d* 0.03, *e* 0.05, and *f* 0.08 Ag-64 with **a** 0.02, **b** 0.05, and **c** 0.08 F127 at 20,000 simulation steps (for clarity, water beads are invisible. PEO, PPO, and SiO are represented in *red*, *purple*, and *blue*, respectively)

core size. Overall, the Ag-64/F127 aggregate becomes larger with the increase of the amounts of F127 and Ag-64. Detailed variation on the conformation of Ag-64/F127 aggregate should be obtained from the root-mean-square end-to-end distance.

Root-mean-square end-to-end distance of Ag-64 and F127

There are requirements in the knowledge of the interaction mechanism which is critical for solution properties and further application. The square root of the mean-square end-to-end distance of a linear polymer chain averages over all conformations of the chain [50]. Therefore, the root-mean-square (RMS) end-to-end distance of Ag-64 and F127 will provide available information on the mechanism of aggregate formation. In Fig. 7, the RMS end-to-end distance of Ag-64 does not change much with increasing $\varphi_{\text{Ag-64}}$, and the curves are basically in an ascending trend. Additionally, the RMS end-to-end distance has an increase after more amounts of F127 are added. From the results in above sections, different types of aggregates form with the variation of Ag-64 and F127 contents. At low volume fractions, F127 threads through one Ag-64 micelle or more to form a pearl-necklace aggregate, as there is more polymer

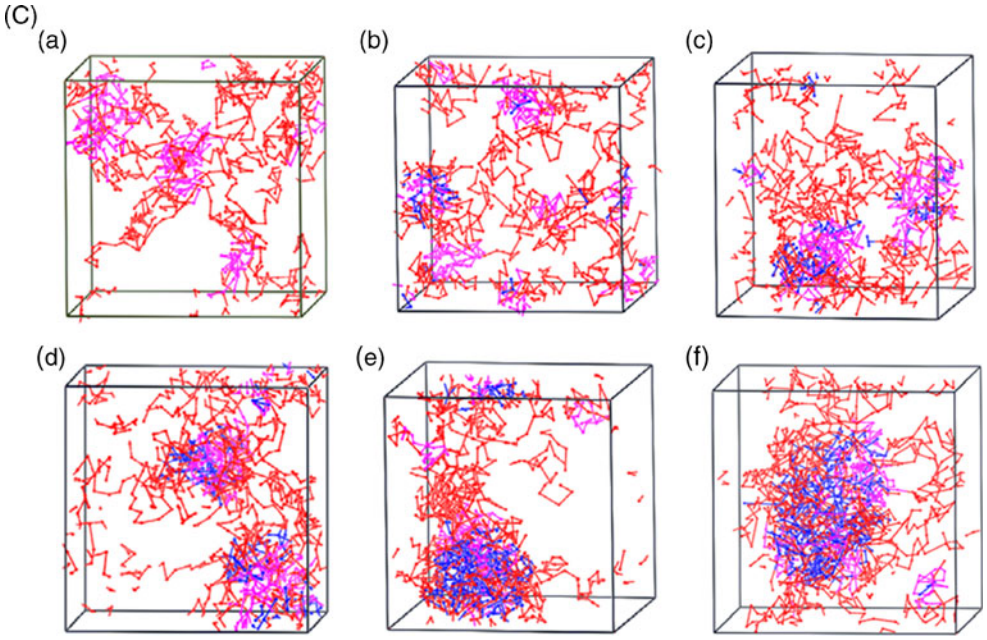

Fig. 4 (continued)

in solution. At high volume fractions, large coil/cluster aggregate appears. In each case, all the Ag-64 molecules adsorb on F127 chains. Thereby, the RMS end-to-end distance of Ag-64 is not affected obviously with the variation of surfactant and polymer contents. It increases a little at higher volume fractions as larger aggregates form.

For F127, the curves vary more obviously which can be determined from the *y*-coordinate values. There is a maximum in the variation curve of F127 RMS end-to-end distance, and it locates at higher $\varphi_{\text{Ag-64}}$ with the increase of φ_{F127} (at 0.02, 0.05, and 0.06, $\varphi_{\text{Ag-64}}$ for the systems contained 0.02, 0.05, and 0.08 F127, respectively). At low

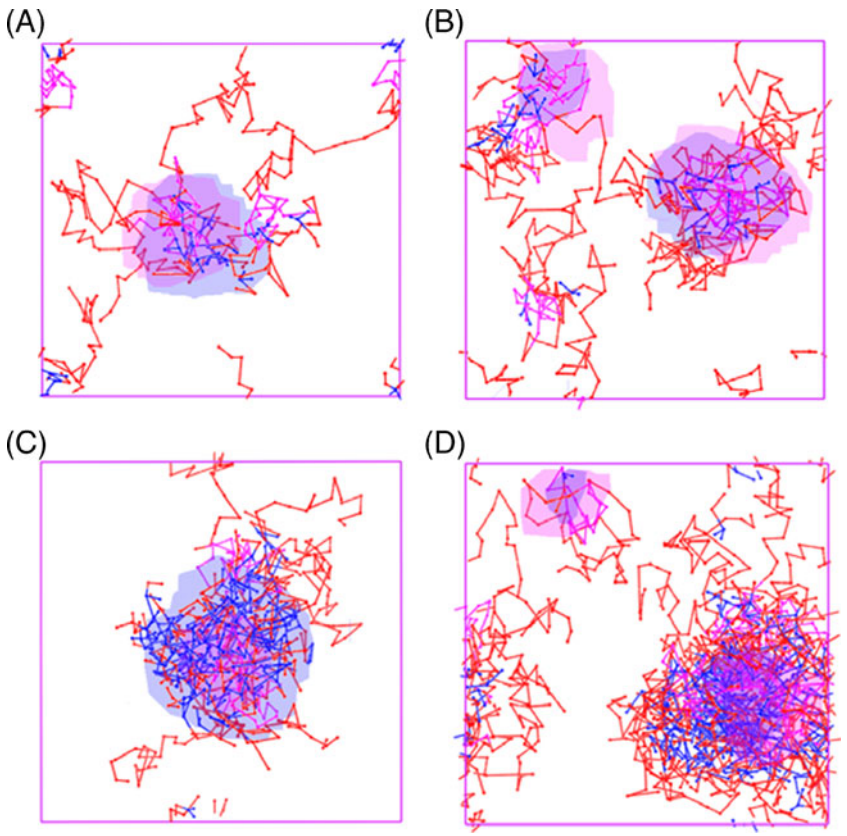

Fig. 5 Distribution profiles of SiO group (displayed in *blue*) and PO group (displayed in *purple*) at different contents of Ag-64 and F127 in aqueous solutions. Water beads are invisible

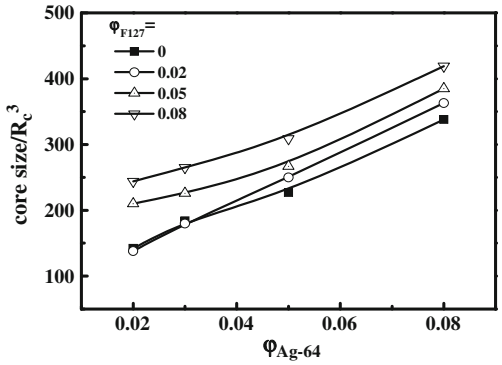

Fig. 6 The variation on the core size of Ag-64/F127 aggregates in the absence and presence of F127 as a function of φ_{Ag-64}

φ_{Ag-64}, hydrophobic segment (PPO group) of F127 is prone to escape from water so that the chain of F127 shrinks corresponding to low RMS end-to-end distance. With the increase of φ_{Ag-64}, the SiO groups of Ag-64 interact with the PPO groups of F127. The binding of Ag-64 to the PPO segment of F127 weakens the hydrophobicity of F127 but strengthens its hydrophilicity. As a result, F127 coil swells leading to the highest RMS end-to-end distance. Comparing Fig. 4a (c) with Fig. 4a (b), more Ag-64 adsorb on F127 so that the polymer chains are more stretched in the solutions. Further increasing φ_{Ag-64}, swollen F127 coils twist with each other, and then the coil/cluster aggregate forms. Therefore, the RMS end-to-end distance of F127 declines and then reaches a plateau. From Fig. 4a (d–f), it can be observed that F127 forms compact aggregates with Ag-64. The RMS end-to-end distance curve of F127 has relatively small variation as φ_{F127} is above 0.02. There are many F127 molecules in all the systems, so that the long chains readily twist with each other, suggesting this impact has great influence on the formation of Ag-64/F127 aggregates. As a result, the RMS end-to-end distance value of polymer has a little change with surfactant content. However, this value is high in the system contained 0.05 F127 and 0.05 Ag-64. In Fig. 4b (e), there is free F127 stretching in water, and it coexists with Ag-64/F127 complex, which could be a transition phase of the coil/cluster aggregate. Thereby, the RMS end-to-end distance of F127 is high in this system.

It can be also observed from Fig. 7b that the plateau value of the RMS end-to-end distance curve of F127 is the lowest as φ_{F127} is 0.02. In this case, the aggregate construction is compact, which can be approved by the fact that the average RMS end-to-end distance value of Ag-64 at this range is the lowest. Contrasting the configuration in Fig. 4a (f) with those in Fig. 4b (f) and c (f) clearly shows a relatively compact construction in the former picture. Large amounts of Ag-64 are in the solutions, and they can compress F127 chains after the adsorption on F127. The polymer chain is more shrunk with the influence of Ag-64 as a little polymer exists. Therefore, the plateau value is bigger as φ_{F127} is beyond 0.02.

From above analysis, there are two main factors contributing to the formation of different Ag-64/F127 aggregates—the hydrophobic interaction and twist of F127 coils. The dominant force of Ag-64 interacting with F127 is the hydrophobic association between SiO group of Ag-64 and PPO group of F127. Ag-64 aggregates on the hydrophobic part of F127 to form a pearl-necklace structure, and the shrinking coil swells. At higher amounts of F127, swollen F127 coils twist together, and the coil/cluster aggregate forms.

From above experimental and simulation results, different aggregates form with the variation of surfactant and polymer contents. The process of aggregate formations and their conformations are illustrated in Fig. 8. As both φ_{Ag-64} and φ_{F127} are low, Ag-64 combines to F127 due to the binding of SiO group to PPO group (Fig. 8a). It is suggested that the interaction between F127 and Ag-64 takes place mainly via hydrophobic interaction between the PO block of F127 and the trisiloxane group of Ag-64. Keeping φ_{F127} constant and increasing φ_{Ag-64}, more Ag-64 molecules aggregate on the chain of F127, and an aggregate forms with F127 as skeleton (Fig. 8b). As φ_{Ag-64} is higher, a lot of Ag-64 adsorbs on twisted F127 chain, and then the coil/cluster aggregate forms (Fig. 8c). If one increases φ_{F127}, a breakdown of aggregate occurs, and F127 threads through some

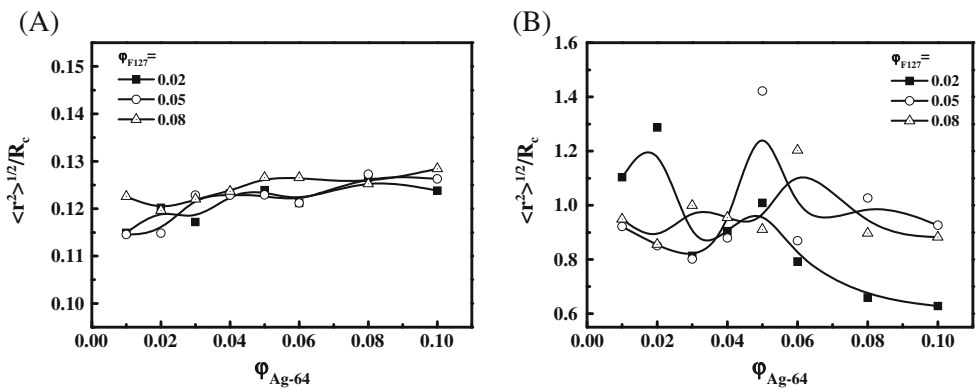

Fig. 7 Root-mean-square end-to-end distance variation of **a** Ag-64 and **b** F127 as a function of φ_{Ag-64}

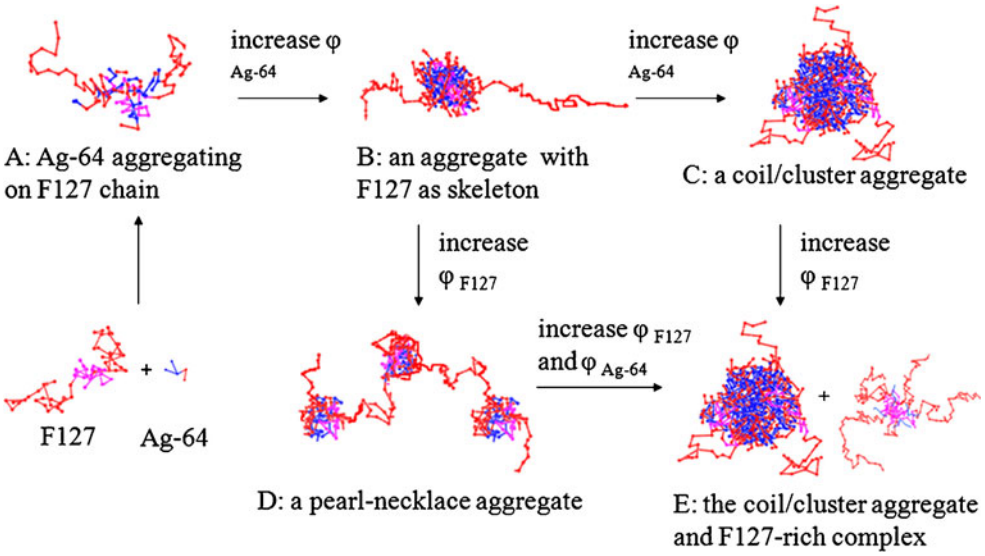

Fig. 8 Conformations of Ag-64/F127 aggregates as a function of volume fraction (φ). PEO, PPO, and SiO are represented in *red*, *purple*, and *blue*, respectively

Ag-64 micelles to form a pearl-necklace aggregate (Fig. 8d). As φ_{F127} is high enough, the F127-rich complex and the coil/cluster aggregate coexist in the solution (Fig. 8e).

Conclusions

The interaction between an ethoxy-modified trisiloxane (a silicone surfactant, named Ag-64) and a block polyether F127 was investigated via experimental investigation and DPD simulation. In the presence of F127, the surface activity and aggregation behavior of Ag-64 change remarkably. From the surface tension results, different types of aggregates may form at the concentrations below T_1, between T_1 and T_2, and beyond T_2 (corresponding to regions I, II, and III, respectively). This presumption is further confirmed via DLS measurement, and the polarity in the micelle of Ag-64 also supports the deduction that F127 coil threads through Ag-64 micelles. Combining all the results obtained by different measurements, it is indicated that unimer or oligomer of F127 appears in region I, Ag-64/F127 aggregate with F127 as skeleton and the pearl-necklace aggregate in which F127 coil threads through Ag-64 micelles are discovered in region II, and coil/cluster aggregate exists in region III.

On the other hand, DPD simulations could give further qualitative support for the formation mechanism of Ag-64/F127 aggregates. It is suggested that two main factors contribute to the aggregate formation, hydrophobic force, and twist of F127 coils. Hydrophobic force is the main factor to cause the binding of Ag-64 to F127. At higher surfactant content, Ag-64 adsorbs onto F127 chain to form an aggregate with F127 as skeleton. Further increasing surfactant content, Ag-64 micelles are strung along the chain of F127. As the amounts of F127 are larger, F127 coils twist together to form coil/cluster aggregates with Ag-64. This research will approach understanding of the interaction between non-ionic surfactants and uncharged water-soluble polymers, and it may provide experimental and theoretical foundations for their further applications.

Acknowledgments We gratefully acknowledge the financial support from the National Natural Science Foundation of China (Grant Nos. 20873077) and the Special Program for Major Research of the Science and Technology, China (Grant Nos. 2011ZX05024-004-08).

References

1. Shiloach A, Blankschtein D (1998) Predicting micellar solution properties of binary surfactant mixtures. Langmuir 14:1618–1636
2. Goddard ED, Ananthapadmanaban KP (1993) Interactions of surfactants with polymer and proteins. CRC Press, Boca Raton
3. Zheng Y, Davis HT (2000) Mixed micelles of nonionic surfactants and uncharged block copolymers in aqueous solutions: microstructure seen by cryo-TEM. Langmuir 16:6453–6459
4. Wu J, Xu Y, Dabros T, Hamza H (2005) Effect of EO and PO positions in nonionic surfactants on surfactant properties and demulsification performance. Colloids Surf A 252:79–85
5. Jain TK, Morales MA, Sahoo SK, Leslie-Pelecky DL, Labhasetwar V (2005) Iron oxide nanoparticles for sustained delivery of anticancer agents. Mol Pharm 2:194–205
6. Hecht E, Mortensen K, Gradzielski M, Hoffmann H (1995) Interaction of ABA block copolymers with ionic surfactants: influence on micellization and gelation. J Phys Chem 99:4866–4874
7. Li Y, Xu R, Couderc S, Bloor M, Wyn-Jones E, Holzwarth JF (2000) Binding of sodium dodecyl sulfate (SDS) to the ABA block copolymer Pluronic F127 ($EO_{97}PO_{69}EO_{97}$): F127 aggregation induced by SDS. Langmuir 17:183–188
8. Cao Q, Zuo C, Li L, He H (2011) Self-assembled nanostructures of bottle-brush polyelectrolytes with oppositely charged surfactants: a computational simulation study. Soft Matter 7:6522–6528
9. Dong SL, Li X, Xu GY, Hoffmann H (2007) A cationic fluorocarbon surfactant DEFUMACl and its mixed systems with cationic surfactants: 19F NMR and surface tension study. J Phys Chem B 111:5903–5910

10. Xin X, Xu GY, Wang YJ, Mao HZ, Zhang ZQ (2008) Interaction between star-like block copolymer and sodium oleate in aqueous solutions. Eur Polym J 44:3246–3255
11. Li YM, Xu GY, Zhua YY, Wang YJ, Gong HJ (2009) Aggregation behavior of Pluronic copolymer in the presence of surfactant: Mesoscopic simulation. Colloids Surf A 334:124–130
12. Anthony O, Zana R (1994) Effect of temperature on the interactions between neutral polymers and a cationic and a nonionic surfactant in aqueous solutions. Langmuir 10:4048–4052
13. Feitosa E, Brown W, Wang K, Barreleiro PCA (2001) Interaction between poly(ethylene glycol) and $C_{12}E_8$ investigated by dynamic light scattering, time-resolved fluorescence quenching, and calorimetry. Macromolecules 35:201–207
14. Feitosa E, Brown W, Vasilescu M, Swanson-Vethamuthu M (1996) Effect of temperature on the interaction between the nonionic surfactant $C_{12}E_5$ and poly(ethylene oxide) investigated by dynamic light scattering and fluorescence methods. Macromolecules 29:6837–6846
15. Löf D, Schillén K, Loh W, Olofsson G (2007) A calorimetry and light scattering study of the formation and shape transition of mixed micelles of $EO_{20}PO_{68}EO_{20}$ triblock copolymer (P123) and nonionic surfactant ($C_{12}EO_6$). J Phys Chem B 111:5911–5920
16. Ohta S, Nitta N, Takahashi M, Sonoda A, Tanaka T, Yamasaki M, Furukawa A, Takazakura R, Murata K, Sakamoto T, Kushibiki T, Tabata Y (2006) Pluronic F127: application in arterial embolization. J Vasc Interv Radiol 17:533–539
17. Xiong XY, Tam KC, Gan LH (2005) Release kinetics of hydrophobic and hydrophilic model drugs from pluronic F127/poly(lactic acid) nanoparticles. J Control Release 103:73–82
18. Dung TH, Kim J, Kim MS, Kim JS, Yoo H (2008) Preparation and biophysical characterization of Pluronic F127-dendrimer conjugate as a delivery agent of antisense oligonucleotides. J Nanosci Nanotechnol 8:5326–5330
19. James-Smith MA, Shekhawat D, Moudgil BM, Shah DO (2007) Determination of drug and fatty acid binding capacity to Pluronic F127 in microemulsions. Langmuir 23:1640–1644
20. Mao C, Liang CX, Mao YQ, Li L, Hou XM, Shen J (2009) Modification of polyethylene with Pluronics F127 for improvement of blood compatibility. Colloids Surf B Biointerfaces 74:362–365
21. Couderc S, Li Y, Bloor DM, Holzwarth JF, Wyn-Jones E (2001) Interaction between the nonionic surfactant hexaethylene glycol mono-n-dodecyl ether ($C_{12}EO_6$) and the surface active nonionic ABA block copolymer pluronic F127 ($EO_{97}PO_{69}EO_{97}$) formation of mixed micelles studied using isothermal titration calorimetry and differential scanning calorimetry. Langmuir 17:4818–4824
22. Ge LL, Guo R, Zhang XH (2008) Formation and microstructure transition of F127/TX-100 complex. J Phys Chem B 112:14566–14577
23. Wang GY, Du ZP, Li QX, Zhang W (2010) Carbohydrate-modified siloxane surfactants and their adsorption and aggregation behavior in aqueous solution. J Phys Chem B 114:6872–6877
24. Pang JY, Xu GY, Tan YB, He F (2010) Water-dispersible carbon nanotubes from a mixture of an ethoxy-modified trisiloxane and pluronic block copolymer F127. Colloid Polym Sci 288:1665–1675
25. Groot RD (2000) Mesoscopic simulation of polymer-surfactant aggregation. Langmuir 16:7493–7502
26. Li YM, Xu GY, Chen YJ, Luan YX, Yuan SL (2006) Computer simulations of surfactants and surfactant/polymer assemblies. Comput Mater Sci 36:386–396
27. Li YM, Xu GY, Luan YX, Yuan SL, Zhang ZQ (2005) Studies on the interaction between tetradecyl dimethyl betaine and sodium carboxymethyl cellulose by DPD simulations. Colloids Surf A 257–258:385–390
28. Li YM, Xu GY, Chen AM, Yuan SL, Cao XR (2005) Aggregation between xanthan and nonyphenyloxypropyl β-hydroxyltrimethylammonium bromide in aqueous solution: MesoDyn simulation and binding isotherm measurement. J Phys Chem B 109:22290–22295
29. Sun HY, Xu GY, Li YM, Chen YJ (2006) Mesoscopic simulation of the aggregation behavior of fluorinated surfactant in aqueous solution. J Fluorine Chem 127:187–192
30. Hoogerbrugge PJ, Koelman JMVA (1992) Simulating microscopic hydrodynamic phenomena with dissipative particle dynamics. Europhys Lett 19:155–160
31. Groot R D, Warren P B (1997) Dissipative particle dynamics: Bridging the gap between atomistic and mesoscopic simulation. J Chem Phys 107
32. Balazs AC, Hu JY (1989) Effects of surfactant concentration on polymer-surfactant interactions in dilute solutions: a computer model. Langmuir 5:1230–1234
33. van Vlimmeren BAC, Maurits NM, Zvelindovsky AV, Sevink GJA, Fraaije JGEM (1999) Simulation of 3D mesoscale structure formation in concentrated aqueous solution of the triblock polymer surfactants $(\text{ethylene oxide})_{13}(\text{propylene oxide})_{30}(\text{ethylene oxide})_{13}$ and $(\text{propylene oxide})_{19}(\text{ethylene oxide})_{33}(\text{propylene oxide})_{19}$. Application of dynamic mean-field density functional theory. Macromolecules 32:646–656
34. Chen S, Guo C, Hu GH, Liu HZ, Liang XF, Wang J, Ma JH, Zheng L (2007) Dissipative particle dynamics simulation of gold nanoparticles stabilization by PEO–PPO–PEO block copolymer micelles. Colloid Polym Sci 285:1543–1552
35. Guo SL, Hou TJ, Xu XJ (2002) Simulation of the phase behavior of the $(EO)_{13}(PO)_{30}(EO)_{13}$(Pluronic L64)/water/*p*-xylene system using MesoDyn. J Phys Chem B 106:11397–11403
36. Alexandridis P, Athanassiou V, Fukuda S, Hatton TA (1994) Surface activity of poly(ethylene oxide)-block-poly(propylene oxide)-block-poly(ethylene oxide) copolymers. Langmuir 10:2604–2612
37. De Lisi R, Milioto S (2000) $\text{Poly(ethylene oxide)}_{13}$-$\text{poly(propylene oxide)}_{30}$-$\text{poly(ethylene oxide)}_{13}$ electrolyte interactions in aqueous solutions at some temperatures. Langmuir 16:5579–5583
38. Ding Y, Wang Y, Guo R (2004) Aggregation properties of amphiphilic poly(ethylene oxide)-poly(propylene oxide)-poly(ethylene oxide) block copolymer studied by cyclic voltammetry. J Surfactant Deterg 7:379–385
39. Folmer BM, Kronberg B (2000) Effect of surfactant-polymer association on the stabilities of foams and thin films: sodium dodecyl sulfate and poly(vinyl pyrrolidone). Langmuir 16:5987–5992
40. Monteux C, Williams CE, Bergeron V (2004) Interfacial microgels formed by oppositely charged polyelectrolytes and surfactants. Part 2. Influence of surfactant chain length and surfactant/polymer ratio. Langmuir 20:5367–5374
41. Taylor DJF, Thomas RK, Li PX, Penfold J (2003) Adsorption of oppositely charged polyelectrolyte/surfactant mixtures. Neutron reflection from alkyl trimethylammonium bromides and sodium poly(styrenesulfonate) at the air/water interface: the effect of surfactant chain length. Langmuir 19:3712–3719
42. Li Y, Xu R, Bloor DM, Holzwarth JF, Wyn-Jones E (2000) The binding of sodium dodecyl sulfate to the ABA block copolymer Pluronic F127 ($EO_{97}PO_{69}EO_{97}$): an electromotive force, microcalorimetry, and light scattering investigation. Langmuir 16:10515–10520
43. Wang G, Olofsson G (1998) Titration calorimetric study of the interaction between ionic surfactants and uncharged polymers in aqueous solution. J Phys Chem B 102:9276–9283
44. Nilsson S, Holmberg C, Sundelöf LO (1995) Aggregation numbers of SDS micelles formed on EHEC. A steady state fluorescence quenching study. Colloid Polym Sci 273:83–95
45. Asakawa T, Okada T, Hayasaka T, Kuwamoto K, Ohta A, Miyagishi S (2006) The unusual micelle micropolarity of partially fluorinated gemini surfactants sensed by pyrene fluorescence. Langmuir 22:6053–6055

46. Li Y, Xu R, Couderc S, Bloor DM, Holzwarth JF, Wyn-Jones E (2001) Binding of tetradecyltrimethylammonium bromide to the ABA block copolymer Pluronic F127 (EO_{97} PO_{69} EO_{97}): electromotive force, microcalorimetry, and light scattering studies. Langmuir 17:5742–5747
47. Cardoso da Silva R, Olofsson G, Schillén K, Loh W (2002) Influence of ionic surfactants on the aggregation of poly (ethylene oxide)-poly(propylene oxide)-poly(ethylene oxide) block copolymers studied by differential scanning and isothermal titration calorimetry. J Phys Chem B 106:1239–1246
48. Jansson J, Schillén K, Olofsson G, Cardoso da Silva R, Loh W (2004) Interaction between PEO-PPO-PEO triblock copolymers and ionic surfactants in aqueous solution studied using light scattering and calorimetry. J Phys Chem B 108:82–92
49. Li Y, Hou T, Guo S, Wang K, Xu X (2000) The Mesodyn simulation of pluronic water mixtures using the 'equivalent chain' method. PCCP 2:2749–2753
50. Lam Y-M, Goldbeck-Wood G (2003) Mesoscale simulation of block copolymers in aqueous solution: parameterisation, micelle growth kinetics and the effect of temperature and concentration morphology. Polymer 44:3593–3605